IRS-assisted communication performance optimization method for shipborne DFRC system

Jielong Lu , Zhenkai Zhang , Boon-Chong Seet , Baiheng Wang

PII: S0165-1684(25)00493-1
DOI: https://doi.org/10.1016/j.sigpro.2025.110377
Reference: SIGPRO 110377

To appear in: *Signal Processing*

Received date: 11 August 2025
Revised date: 29 September 2025
Accepted date: 29 October 2025

Please cite this article as: Jielong Lu , Zhenkai Zhang , Boon-Chong Seet , Baiheng Wang , IRS-assisted communication performance optimization method for shipborne DFRC system, *Signal Processing* (2025), doi: https://doi.org/10.1016/j.sigpro.2025.110377

IRS-assisted communication performance optimization method for shipborne DFRC system

Jielong Lu [1], Zhenkai Zhang [1*], Boon-Chong Seet [2], Baiheng Wang [1]

1: Jiangsu University of Science and Technology, Ocean College, Zhenjiang 212028, China

2: Department of Electrical and Electronic Engineering, Auckland University of Technology, Auckland 1010, New Zealand

Abstract

Dual-functional radar-communication (DFRC) has emerged as an effective solution in recent years to address spectrum scarcity in maritime environments, enabling efficient integrated communication and sensing. To mitigate path loss over complex sea surfaces, the intelligent reflecting surface (IRS) is introduced into DFRC systems, enhancing signal quality by providing an additional propagation path. To address the impact of sea wave fluctuations on the communication channel of maritime vessels, an alternating optimization (AO) algorithm based on semidefinite relaxation and fractional programming (SDR-FP) is proposed. First, the non-ideal channel state information (CSI) is modeled using a bounded channel uncertainty model via the S-procedure. Second, under constraints on radar detection performance and transmit power, the problem is formulated to maximize the communication sum-rate. Next, the proposed AO algorithm decomposes the original high-dimensional problem into two low-complexity subproblems. Finally, a minimization algorithm is applied to reformulate the non-convex subproblem into a tractable quadratically constrained quadratic program (QCQP). Simulation results demonstrate that the proposed method significantly enhances the communication sum-rate while achieving faster convergence compared to benchmarks.

Keywords: Intelligent reflecting surface, dual-function radar communication, communication and rate, alternating optimization.

1. Introduction

Against the backdrop of growing maritime communication demands, traditional vessel-mounted radar and communication systems typically require separate deployment. This approach poses significant challenges, including hardware duplication, intense competition for spectrum resources, and excessive power consumption. Dual-functional radar-communication (DFRC) systems offer an efficient solution for vessel-mounted platforms by

Corresponding author.

E-mail address: zhangzhenkai@just.edu.cn (Z. Zhang).

integrating radar sensing and wireless communication functionalities onto a single integrated platform [1, 2].

To enable the joint design of radar and communication functionalities, extensive research has been conducted on interference cancellation techniques and integrated beamforming strategies [3]. In [4], an OOK-chirp based radar-communication coexistence (RCC) system was designed. By employing a fixed full-band and a variable sub-band scheme, the system enables low-complexity communication demodulation and same-slope interference cancellation. In [5], a robust joint waveform and filter design model was proposed, which minimizes radiation power and integrates semi-definite programming with alternating optimization (AO) methods to achieve excellent low-probability-of-intercept (LPI) performance and anti-jamming capability under target position uncertainty. By employing efficient resource allocation strategies, the target tracking accuracy can be significantly improved while reducing the overall system energy consumption [6]. Unlike RCC systems, DFRC systems, where radar and communication share the same hardware platform and transmit waveform, offer superior interference management capabilities and greater potential for performance balancing [8,9]. The waveform design in [10] maximizes the radar output signal-to-interference-plus-noise ratio (SINR) by constraining the worst-case reception quality of communication users. The problem is solved using a combination of the coordinate descent method and the Dinkelbach algorithm. In [11], a multicarrier DFRC beamforming scheme with sidelobe-controlled information embedding was designed. A fractional programming-based optimization algorithm was developed for efficient solution. The waveform design in [12] integrates the Cramér–Rao bound (CRB) for radar parameter estimation with the sum rate of communication services in a bistatic DFRC system. A unified fractional programming framework is constructed to efficiently solve the resulting complex non-convex optimization problem. In [13], DFRC system with imperfect channel state information (CSI) is considered, where a robust joint design method for the transmit waveform and receive filter is proposed. The studies above primarily optimize the detection performance of integrated systems. To further investigate the optimization of sensing and communication performance in DFRC systems, radar and communication centric strategies based on joint transmit and receive beamforming are employed, enabling low-complexity approaches to approximate the performance limits [14,15]. Collectively, these studies advance DFRC system development through diverse technical pathways, improving interference management, performance optimization, and integrated design.

Deploying Intelligent Reflecting Surfaces (IRS) within DFRC systems introduces additional reflection paths, thereby enhancing both communication and sensing performance [16-18]. In [19], a DFRC system with an active RIS was investigated, where the joint design of the base station beamforming and RIS reflection coefficients enhances the secrecy rate under given constraints, and it was demonstrated that the active RIS outperforms the

passive RIS in mitigating multiplicative fading and improving overall performance. In [20], an active IRS-assisted DFRC system is designed to significantly improve the system's secrecy rate under radar sensing constraints, effectively overcoming the multiplicative fading effects of multi-hop channels. In [21], a super-diagonal IRS-assisted DFRC system is proposed, where the reflection and transmission modes overcome the conventional half-space limitation to achieve full-space coverage, significantly enhancing communication performance under strong clutter conditions. In [22], an IRS-assisted millimeter-wave integrated sensing and communication (ISAC) system was proposed, where the joint optimization of the communication beamforming vector and IRS phase shifts enables simultaneous enhancement of the communication rate and multi-target detection, verifying the effectiveness of IRS in improving ISAC system performance. The above research mainly focuses on enhancing the single-target performance of either communication or radar. To further explore the potential of IRS in system level integrated sensing and communication optimization [23], the scheme in [24] achieves simultaneous enhancement of multicast capacity and sensing accuracy by optimizing target scheduling, beamforming, reflection coefficients and unmanned aerial vehicle (UAV) trajectory in a unified manner, providing a novel framework for dynamic integrated sensing and communication systems. In [25], a joint optimization framework for IRS-assisted radar-communication is proposed, enabling low-complexity joint beamforming without dedicated radar signals. A novel SDR-based reconstruction algorithm is employed to reduce system outage probability under cross-correlation constraints, effectively overcoming the limitations of passive beam design. IRS can also enhance the energy efficiency of the system [26]. By employing a novel joint resource optimization approach, both the system's energy efficiency and the users' weighted sum rate can be significantly improved [27,28]. In [29], an energy-efficient optimization scheme for IRS-assisted DFRC systems is developed, where beamforming and phase shift matrices are jointly designed under both perfect and imperfect CSI. This approach significantly enhances communication energy efficiency while satisfying stringent radar performance constraints. Although these studies advance interference management, performance optimization, and integrated design in DFRC systems, they primarily focus on terrestrial environments, with research on maritime applications remaining insufficient.

To explore the potential of IRS in maritime integrated sensing and communication systems [30], a scheme based on reconfigurable reflecting array (RRA) is developed in [31], which jointly optimizes beamforming and service time allocation. This approach significantly enhances the effective sum rate of maritime communications while maintaining reliable performance and substantially reducing hardware complexity and deployment cost. In [32], a robust joint beamforming design is proposed for IRS-assisted maritime non-orthogonal multiple access (NOMA) systems. By innovatively integrating the S-procedure with an AO technique, the method effectively

handles channel uncertainty constraints, significantly reduces the base station transmit power, and ensures the worst-case rate requirements. The study in [33] maximizes the system's energy efficiency by integrating the Dinkelbach method with a mean square error-based approach. This design significantly enhances energy efficiency performance while ensuring the communication and illumination requirements of maritime vessels are satisfied. However, the study primarily focuses on maritime communication systems and does not consider sensing functionalities. In [34], a maritime communication framework that synergistically integrates IRS with active relays is proposed. Through the combined optimization of relay mode dynamic switching, power control, and active-passive beamforming, the scheme significantly reduces overall system power consumption while ensuring quality of service for vessels. The genetic algorithm with an improved elite retention strategy in [35] accelerates convergence through individual handling mechanisms and enhanced elite preservation, thereby optimizing the sensing performance of the maritime DFRC system. These studies have made progress in integrated designs for interference suppression, robustness enhancement, and resource allocation in maritime joint sensing and communication systems but overlook the complex and dynamic characteristics of the marine environment.

The aforementioned studies have conducted in-depth research on IRS-assisted radar and communication coexistence systems and achieved significant breakthroughs. However, maritime environments often pose greater challenges to the channels. Most of these works focus on static sea scenarios and optimize DFRC systems under the assumption of ideal CSI, without considering the impact of complex sea conditions. Therefore, addressing the optimization of the communication sum rate for communication ships in dynamic maritime environments within IRS-assisted DFRC systems, the self-interference problem caused by IRS reflections, and the need for reflection power control in IRS-equipped unmanned surface vessels. To address these challenges, this paper investigates the optimization of communication performance in IRS-assisted shipborne DFRC systems. An AO algorithm based on semidefinite relaxation and fractional programming (SDR-FP) is proposed to improve both communication rate and radar sensing performance under the constraints of communication quality, radar detection, and transmit power. The key contributions of this study include:

1）Accounting for the impact of sea wave fluctuations in the maritime environment, the CSI errors caused by such dynamics are modeled as a bounded uncertainty through analytical derivation. This modeling facilitates the design of both transmit and reflective beamforming strategies, thereby enhancing the communication reliability of the DFRC system.

2）Under the imperfect channel state information (CSI) scenario, this paper investigates the communication performance optimization for an IRS-assisted shipborne DFRC system. By employing the S-procedure to handle

the bounded channel uncertainty model, an AO algorithm based on SDR-FP is proposed, which effectively enhances the communication performance of the DFRC system.

3）For a given transmit precoding matrix, the majorization-minimization (MM) algorithm is employed to transform the non-convex unit-modulus constrained problem into a quadratically constrained quadratic programming (QCQP) problem. Meanwhile, self-interference cancellation techniques are applied to effectively suppress the self-interference of echo signals between the radar and IRS.

The remainder of this paper is organized as follows: Section 2 introduces the system model formulation and the computation of the bounded unstable CSI model. Section 3 outlines the proposed algorithm. Section 4 presents simulation experiments and results analysis of the proposed algorithm. Section 5 concludes with a summary of the main work of this paper.

Symbol description： $\|\cdot\|_2$ and $\|\cdot\|_F$ denote the spectral norm and Frobenius norm of a matrix respectively; $(\cdot)^T$ and $(\cdot)^H$ denote the transpose and conjugate transpose of a vector or matrix, respectively; $\mathrm{tr}(\cdot)$ denotes the trace of a matrix; $\succeq$ indicates that a matrix is positive semidefinite; $\odot$ and $\otimes$ denote the Hadamard product and Kronecker product, respectively; $\mathbb{C}^{L\times 1}$ denotes the set of complex $L\times 1$ vectors;; $\mathcal{CN}$ denotes the Gaussian distribution; $\mathrm{Re}(\cdot)$ denotes the real part of the complex number in parentheses.

2. System model

As illustrated in Fig. 1, this paper investigates an IRS-assisted shipborne integrated radar-communication system comprising an unmanned surface vessel equipped with an IRS, a radar target, K communication ships, and a vessel equipped with a DFRC transmitter. The communication ships are situated in a dynamic maritime environment subject to sea wave fluctuations, resulting in time-varying azimuth angles for the links between each user and both the DFRC transmitter and the IRS. The DFRC transmitter is equipped with M antennas to simultaneously serve the communication ships and detect the radar target, while the IRS possesses L reflecting elements.

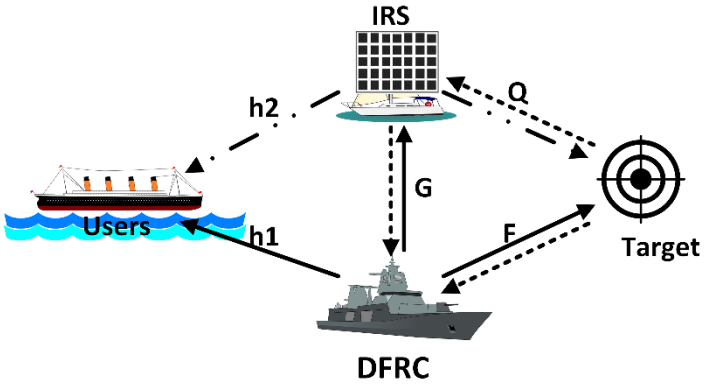

Fig. 1 IRS-assisted integrated radar and communication system

The temporal random variations in azimuth angles $\theta_{1,k}$ and $\theta_{2,k}$ between the DFRC-to-kth-user and IRS-to-kth-user paths introduce CSI error into the DFRC transmitter's beamforming design. Given the bounded angular variation range in this model, the actual azimuth angles $\theta_{1,k}$ and $\theta_{2,k}$ can be written as

$$\theta_{1,k} = \bar{\theta}_{1,k} + \Delta\theta_{1,k}, k \in K \tag{1}$$

$$\theta_{2,k} = \bar{\theta}_{2,k} + \Delta\theta_{2,k}, k \in K \tag{2}$$

where $\bar{\theta}_{1,k}$ and $\bar{\theta}_{2,k}$ are estimates of $\theta_{1,k}$ and $\theta_{2,k}$, respectively, $\Delta\theta_{1,k}$ and $\Delta\theta_{2,k}$ represent angular variations satisfying $|\Delta\theta_{1,k}| \le \vartheta_1$ and $|\Delta\theta_{2,k}| \le \vartheta_2$, respectively, ϑ_1 and ϑ_2 denoting maximum angular variations [32].

Therefore, the channel from the base station to the *k*-th user can be written as

$$\boldsymbol{h}_{1,k}^H = \bar{\boldsymbol{h}}_{1,k}^H + \Delta\boldsymbol{h}_{1,k}^H, k \in K \tag{3}$$

$$\boldsymbol{h}_{2,k}^H = \bar{\boldsymbol{h}}_{2,k}^H + \Delta\boldsymbol{h}_{2,k}^H, k \in K \tag{4}$$

where $\bar{\boldsymbol{h}}_{1,k}^H$ and $\bar{\boldsymbol{h}}_{2,k}^H$ represent estimates of $\boldsymbol{h}_{1,k}^H \in \mathbb{C}^{1\times M}$ and $\boldsymbol{h}_{2,k}^H \in \mathbb{C}^{1\times L}$ respectively, while $\Delta\boldsymbol{h}_{1,k}$ and $\Delta\boldsymbol{h}_{2,k}^H$ denote CSI errors induced by sea wave fluctuations. All considered links incorporate both line-of-sight (LOS) and non-line-of-sight (NLOS) components in the maritime environment, accounting for both large-scale and small-scale fading effects. The $\bar{\boldsymbol{h}}_{1,k}^H$ can be expressed as:

$$\boldsymbol{h}_{1,k}^H = \sqrt{\frac{\xi(d_{1,k})K_1}{1+K_1}}\bar{\boldsymbol{h}}_{1,k,\mathrm{L}}^H + \sqrt{\frac{\xi(d_{1,k})}{1+K_1}}\boldsymbol{h}_{1,k,\mathrm{N}}^H \tag{5}$$

where $\bar{\boldsymbol{h}}_{1,k,\mathrm{L}}^H \in \mathbb{C}^{1\times M}$ represents the LOS component of $\bar{\boldsymbol{h}}_{1,k}^H$, K_1 is the Rician fading factor of the direct link between the DFRC transmitter and the user, $\boldsymbol{h}_{1,k,\mathrm{N}}^H$ denotes the NLOS component of $\bar{\boldsymbol{h}}_{1,k}^H$ following $\mathcal{CN}(0,1)$, $\xi(d_{1,k})$ represents the channel power gain from large-scale fading, $d_{1,k}$ is the distance from the DFRC transmitter to the *k*-th user, and $\bar{\boldsymbol{h}}_{1,k,\mathrm{L}}^H$ can be written as:

$$\bar{\boldsymbol{h}}_{1,k,\mathrm{L}}^{H}=[1,e^{-j(\frac{2\pi b_{1,k}}{\lambda_{1,k}})\sin\bar{\theta}_{1,k}},...,e^{-j(\frac{2\pi b_{1,k}(M-1)}{\lambda_{1,k}})\sin\bar{\theta}_{1,k}}] \tag{6}$$

where $b_{1,k}$ denotes propagation distance and $\lambda_{1,k}$ represents carrier wavelength.

Through first-order Taylor expansion, CSI error $\Delta\boldsymbol{h}_{1,k}^{H}\in\mathbb{C}^{1\times M}$ can be written as:

$$\Delta\boldsymbol{h}_{1,k}^{H}=\sqrt{\frac{\xi(d_{1,k})K_1}{1+K_1}}\bar{\boldsymbol{h}}_{1,k,\mathrm{L}}^{H}\odot(1,-j\frac{2\pi b_{1,k}\cos\bar{\theta}_{1,k}}{\lambda_{1,k}},...,-j\frac{2\pi b_{1,k}(M-1)\cos\bar{\theta}_{1,k}}{\lambda_{1,k}})\Delta\theta_{1,k} \tag{7}$$

The channel errors between the communication ship (k-th user) and DFRC transmitter are assumed to satisfy:

$$\left\|\Delta\boldsymbol{h}_{1,k}^{H}\right\|_2=\left\|a_k\Delta\theta_{1,k}\right\|_2\le\vartheta_1\left\|a_k\right\|_2=\varpi_1 \tag{8}$$

where $a_k=\sqrt{\frac{\xi(d_{1,k})K_1}{1+K_1}}\bar{\boldsymbol{h}}_{1,k,\mathrm{L}}^{H}\odot(1,-j\frac{2\pi b_{1,k}\cos\bar{\theta}_{1,k}}{\lambda_{1,k}},...,-j\frac{2\pi b_{1,k}(M-1)\cos\bar{\theta}_{1,k}}{\lambda_{1,k}})$.

Similarly, the channel errors between the communication ship and the IRS are assumed to satisfy:

$$\left\|\Delta\boldsymbol{h}_{2,k}^{H}\right\|_2=\left\|b_k\Delta\theta_{2,k}\right\|_2\le\vartheta_2\left\|b_k\right\|_2=\varpi_2 \tag{9}$$

where $b_k=\sqrt{\frac{\xi(d_{2,k})K_2}{1+K_2}}\bar{\boldsymbol{h}}_{2,k,\mathrm{L}}^{H}\odot(1,-j\frac{2\pi b_{2,k}\cos\bar{\theta}_{2,k}}{\lambda_{2,k}},...,-j\frac{2\pi b_{2,k}(M-1)\cos\bar{\theta}_{2,k}}{\lambda_{2,k}})$.

Each passive reflecting element of the IRS reflects incident signals with desired phase shifts and amplitude reflection coefficients. The reflection coefficient matrix can be expressed as $\boldsymbol{\Xi}=\mathrm{diag}(\Psi_1\exp(\mathrm{j}\theta_I),...,\Psi_{\mathrm{L}}\exp(\mathrm{j}\theta_L))\in\mathbb{C}^{L\times L}$, where Ψ_1 denotes the amplitude attenuation vector and θ_L represents the phase shift vector. Implementing element-level joint amplitude-phase control incurs substantial hardware costs, thus all elements typically maintain uniform amplitude with $\Psi_l=1, l\in[1,L]$, Given the IRS deployment on unmanned surface vessels, this work additionally accounts for IRS thermal noise and power consumption. The reflected signal can be formulated as [36]:

$$\boldsymbol{y}_{\mathrm{I}}=\boldsymbol{\Xi}^{H}\boldsymbol{G}\boldsymbol{w}\boldsymbol{x}+\boldsymbol{\Xi}\boldsymbol{Q}\boldsymbol{\Xi}^{H}\boldsymbol{G}\boldsymbol{w}\boldsymbol{x}+\boldsymbol{\Xi}n_I \tag{10}$$

where $\boldsymbol{x}$ denotes the transmitted signal at the DFRC, $\boldsymbol{w}\in\mathbb{C}^{M\times 1}$ represents the beamforming vector of the DFRC transmitter, and $n_I\sim\mathcal{CN}(0,\sigma_{\mathrm{I}}^2\mathrm{I}_{\mathrm{L}})$ signifies additive white Gaussian noise (AWGN) at the IRS with noise power of σ_{I}^2.

Since echo signals from the DFRC-IRS-DFRC link contain no target information and constitute interference for target sensing, the radar signal at the DFRC receiver can be expressed as:

$$\boldsymbol{y}_{\mathrm{r}}=(\boldsymbol{G}^{H}\boldsymbol{\Xi}\boldsymbol{Q}\boldsymbol{\Xi}^{H}\boldsymbol{G}+\boldsymbol{F})\boldsymbol{w}\boldsymbol{x}+\boldsymbol{G}^{H}\boldsymbol{\Xi}^{H}\boldsymbol{G}\boldsymbol{w}\boldsymbol{x}+\boldsymbol{G}^{H}\boldsymbol{\Xi}n_I+n_D \tag{11}$$

where $n_D\sim\mathcal{CN}(0,\sigma_{\mathrm{D}}^2\mathrm{I}_{\mathrm{M}})$ denotes AWGN at the DFRC receiver with noise power σ_{D}^2, $\boldsymbol{G}\in\mathbb{C}^{M\times L}$ represents the maritime channel between the DFRC transmitter and IRS, $\boldsymbol{F}=\varepsilon\boldsymbol{\partial}(\theta)\boldsymbol{\partial}^{\mathrm{H}}(\theta)\in\mathbb{C}^{M\times M}$ is the target response matrix where ε denotes reflection coefficient, $\boldsymbol{\partial}(\theta)\in\mathbb{C}^{N\times 1}$ signifies the antenna array steering vector, and θ indicates the

sensing target angle. Similarly: $\boldsymbol{Q} \in \mathbb{C}^{L\times L}$ constitutes the IRS-to-target response matrix. $\boldsymbol{G}^H \Xi^H \boldsymbol{G}$ represents the self-interference (SI) signal originating from the integrated signal transmitted via the DFRC-IRS path after single reflection, while the IRS-target-IRS-DFRC link signal is omitted due to weak signal strength after multiple reflections [37]. Consequently, after applying effective self-interference cancellation techniques, the received radar signal becomes:

$$\boldsymbol{y}_{\mathrm{r}} = (\boldsymbol{G}^H \boldsymbol{\Xi}\boldsymbol{Q}\boldsymbol{\Xi}^H \boldsymbol{G} + \boldsymbol{F})\boldsymbol{w}\boldsymbol{x} + \mu \boldsymbol{G}^H \boldsymbol{\Xi}^H \boldsymbol{G}\boldsymbol{w}\boldsymbol{x} + \boldsymbol{G}^H \boldsymbol{\Xi} n_I + n_D \tag{12}$$

where μ denotes the mitigated SI coefficient. Therefore, the radar SINR can be written as [38]:

$$\mathrm{SINR}_{\mathrm{r}} = \mathrm{tr}\left(\boldsymbol{A}\boldsymbol{S}\boldsymbol{A}^{\mathrm{H}} \left(\boldsymbol{Z}\right)^{-1}\right) \tag{13}$$

where $\boldsymbol{S} = \boldsymbol{w}\boldsymbol{w}^H$, $\boldsymbol{A} = \boldsymbol{G}^H \boldsymbol{\Xi}\boldsymbol{Q}\boldsymbol{\Xi}^H \boldsymbol{G} + \boldsymbol{F}$, $\boldsymbol{Z} = \mu^2 \boldsymbol{G}^H \boldsymbol{\Xi}^H \boldsymbol{G}\boldsymbol{S}\boldsymbol{G}^H \boldsymbol{\Xi}\boldsymbol{G} + \sigma_{\mathrm{I}}^2 \left(\boldsymbol{G}^H \boldsymbol{\Xi}\right)\left(\boldsymbol{G}^H \boldsymbol{\Xi}\right)^H + \sigma_{\mathrm{D}}^2 \boldsymbol{I}_M$.

The communication ship (k-th user) receives the combined signal from the DFRC transmitter as well as the reflection from the IRS. Since the signal reflected via the target to the communication ship is relatively weak, it can be neglected. Accordingly, the received signal at the *k*-th communication ship can be written as:

$$\boldsymbol{y}_{\mathrm{c},k} = (\boldsymbol{h}_{2,k}{}^{\mathrm{H}} \boldsymbol{\Xi}\boldsymbol{G} + \boldsymbol{h}_{1,k}{}^{\mathrm{H}})\boldsymbol{w}\boldsymbol{x} + \bar{\boldsymbol{h}}_{2,k}^{\mathrm{H}} \boldsymbol{\Xi} n_I + n_C, k \in \mathrm{K} \tag{14}$$

where $n_C \sim \mathcal{CN}(0, \sigma_C^2 \mathrm{I})$ denotes AWGN at the communication ship receiver with noise power σ_C^2 , and the SINR for the *k*-th communication ship is:

$$\mathrm{SINR}_{\mathrm{c},k} = \frac{\boldsymbol{h}_k^{\mathrm{H}} \boldsymbol{S}\boldsymbol{h}_k}{\sigma_{\mathrm{I}}^2 \bar{\boldsymbol{h}}_{2,k}^{\mathrm{H}} \boldsymbol{\Xi}\boldsymbol{\Xi}^{\mathrm{H}} \bar{\boldsymbol{h}}_{2,k} + \sigma_C^2} \tag{15}$$

where $\boldsymbol{h}_k = \boldsymbol{h}_{2,k}^{\mathrm{H}} \boldsymbol{\Xi}\mathbf{G} + \boldsymbol{h}_{1,k}^{\mathrm{H}}, k \in K$, the system's communication sum rate can be written as:

$$R_U = \sum_k^K \log_2\left(1 + \mathrm{SINR}_{\mathrm{c},k}\right) \tag{16}$$

3. Communication performance optimization based on SDR-FP

3.1. Algorithm design

This paper aims to maximize the communication sum rate by jointly optimizing the DFRC transmit beamforming vector $\boldsymbol{w}$ and IRS reflection matrix $\boldsymbol{\Xi}$ under constraints of total transmit power, radar sensing performance, IRS reflection coefficients, and transmit power. With $\boldsymbol{p} = \left[\exp(\mathrm{j}\theta_1), \exp(\mathrm{j}\theta_2), ..., \exp(\mathrm{j}\theta_{\mathrm{L}})\right] \in \mathbb{C}^{1\times \mathrm{L}}$ denoting total power $\boldsymbol{\Xi} = diag\left(\boldsymbol{p}\right)$, the optimization problem is formulated as:

$$
\begin{aligned}
&\max_{\boldsymbol{w},\boldsymbol{p}} \ R_U \\
&s.t. \quad \text{C1:} \min_{\substack{\left\|\Delta \boldsymbol{h}_{1,k}^H\right\|_2 \le \varpi_1 \\ \left\|\Delta \boldsymbol{h}_{2,k}^H\right\|_2 \le \varpi_2}} \ \mathrm{SINR}_{\mathrm{c},k} \ge \gamma_c, k = 1,...,\mathrm{K}, \\
&\quad \text{C2:SINR}_r \ge \gamma_r \\
&\quad \text{C3: tr}\left(\boldsymbol{w}\boldsymbol{w}^{\mathrm{H}}\right) \le \mathrm{P_B}, \\
&\quad \text{C4: } \mathbb{E}\left[\left\|\boldsymbol{y}_{\mathrm{I}}\right\|_2^2\right] \le \mathrm{P_{IRS}}, \\
&\quad \text{C5: } \left|\exp(\mathrm{j}\theta_l)\right|^2 = 1, \ \ l = 1,...,\mathrm{L}
\end{aligned}
\tag{17}
$$

Here, γ_c is the SINR required by the user, and γ_r is the SINR required by the radar. Constraints C1 and C2 represent the communication and radar performance constraints, respectively. Constraint C3 limits the transmit power of the base station. Constraint C4 restricts the maximum reflection power of the IRS. Constraint C5 is the reflection coefficients constraint.

To address the non-convex problem in (17), this study proposes an optimization methodology integrating SDR, FP, AO, and the MM framework. First, the original high-dimensional optimization problem is decomposed into two low-complexity subproblems. Then, the non-convex objective functions in each subproblem are approximated as convex problems using the SDR algorithm and the FP method, respectively. Finally, the problems are solved iteratively until convergence is achieved.

3.2. Optimizing the DFRC beamforming vector w

The objective function (17) can be rewritten as:

$$
\begin{aligned}
&\max_{\boldsymbol{w}} \ R_U \\
&s.t. \quad \text{C1, C2, C3, C4}
\end{aligned}
\tag{18}
$$

Since constraint C1 involves an infinite number of inequality constraints over variables $\Delta \boldsymbol{h}_{1,k}^H$ and $\Delta \boldsymbol{h}_{2,k}^H$, the optimization problem in (18) becomes difficult to solve directly. To address this issue, this paper employs the S-Procedure to convert the infinite constraints into a finite set of constraints.

Lemma 1 [32]: Assume $f_i(\mathrm{x}) \triangleq \boldsymbol{x}^H \boldsymbol{U}_i \boldsymbol{x} + 2\mathrm{Re}\left\{\boldsymbol{u}_i^H \mathrm{x}\right\} + \boldsymbol{u}_i$, where the Hermitian matrix is $\boldsymbol{U}_i \in \mathbb{C}^{L \times L}$, the vector is $\boldsymbol{u}_i \in \mathbb{C}^{L \times 1}$, the scalar is $\boldsymbol{u}_i, i = 1,...,R$, the variable is $\boldsymbol{x} \in \mathbb{C}^{L \times 1}$, then $\left\{ f_i(\boldsymbol{x}) \ge 0 \right\}_{i=1}^R \Rightarrow f_0(\boldsymbol{x}) \ge 0$ holds if and only if there exists $\boldsymbol{\lambda}_i \ge 0, i \in [1, R]$, such that:

$$
\begin{bmatrix} \boldsymbol{U}_0 & \boldsymbol{u}_0 \\ \boldsymbol{u}_0^H & \boldsymbol{u}_0 \end{bmatrix} - \sum_{i=1}^{R} \lambda_i \begin{bmatrix} \boldsymbol{U}_0 & \boldsymbol{u}_i \\ \boldsymbol{u}_i^H & \boldsymbol{u}_i \end{bmatrix} \succeq 0
\tag{19}
$$

In order to rewrite the constraint to the form applicable to Lemma 1, the constraint C1 can be rewritten to

$$\begin{aligned}
&\boldsymbol{h}_{1,k}^H \boldsymbol{S}\boldsymbol{h}_{1,k} - \gamma_c\left(\sigma_1^2 \bar{\boldsymbol{h}}_{2,k}^H \boldsymbol{\Xi}\boldsymbol{\Xi}^H \bar{\boldsymbol{h}}_{2,k} + \sigma_C^2\right) \geq 0,\\
&\mathrm{vec}^H \Delta\boldsymbol{h}_{1,k}^H (-I_M)\mathrm{vec}\Delta\boldsymbol{h}_{2,k}^H + \varpi_1^2 \geq 0,\\
&\forall \mathrm{vec}^H(\mathrm{diag}(\Delta\boldsymbol{h}_{2,k}^H)G)(-I_{ML})\mathrm{vec}(\mathrm{diag}(\Delta\boldsymbol{h}_{2,k}^H)G) + \varpi_3^2 \geq 0.
\end{aligned} \tag{20}$$

where $\left\|\mathrm{diag}(\Delta\boldsymbol{h}_{2,k}^H)G\right\|_F \leq \varpi_3$.

Define $c = \gamma_c\left(\sigma_1^2 \bar{\boldsymbol{h}}_{2,k}^H \boldsymbol{\Xi}\boldsymbol{\Xi}^H \bar{\boldsymbol{h}}_{2,k} + \sigma_C^2\right)$, $\bar{\boldsymbol{P}} = \bar{\boldsymbol{p}}^H \bar{\boldsymbol{p}}, \bar{\boldsymbol{p}} = [\boldsymbol{p}, 1] \in \mathbb{C}^{1\times(L+1)}$, the first line of (20) can be transformed to

$$\begin{aligned}
&\mathrm{tr}\left(\boldsymbol{S}\begin{bmatrix}\mathrm{diag}(\Delta\boldsymbol{h}_{2,k}^H)G\\ \Delta\boldsymbol{h}_{1,k}^H\end{bmatrix}^H \bar{\boldsymbol{P}}\begin{bmatrix}\mathrm{diag}(\Delta\boldsymbol{h}_{2,k}^H)G\\ \Delta\boldsymbol{h}_{1,k}^H\end{bmatrix}\right) + \mathrm{tr}\left(\boldsymbol{S}\begin{bmatrix}\mathrm{diag}(\Delta\boldsymbol{h}_{2,k}^H)G\\ \Delta\boldsymbol{h}_{1,k}^H\end{bmatrix}^H \bar{\boldsymbol{P}}\begin{bmatrix}\mathrm{diag}(\bar{\boldsymbol{h}}_{2,k}^H)G\\ \bar{\boldsymbol{h}}_{1,k}^H\end{bmatrix}\right)\\
&+\mathrm{tr}\left(\boldsymbol{S}\begin{bmatrix}\mathrm{diag}(\bar{\boldsymbol{h}}_{2,k}^H)G\\ \bar{\boldsymbol{h}}_{1,k}^H\end{bmatrix}^H \bar{\boldsymbol{P}}\begin{bmatrix}\mathrm{diag}(\Delta\boldsymbol{h}_{2,k}^H)G\\ \Delta\boldsymbol{h}_{1,k}^H\end{bmatrix}\right) + \mathrm{tr}\left(\boldsymbol{S}\begin{bmatrix}\mathrm{diag}(\bar{\boldsymbol{h}}_{2,k}^H)G\\ \bar{\boldsymbol{h}}_{1,k}^H\end{bmatrix}^H \bar{\boldsymbol{P}}\begin{bmatrix}\mathrm{diag}(\bar{\boldsymbol{h}}_{2,k}^H)G\\ \bar{\boldsymbol{h}}_{1,k}^H\end{bmatrix}\right)\\
&-c \geq 0
\end{aligned} \tag{21}$$

Based on the definition $tr\left(\mathrm{A}^H\mathrm{B}\right) = \mathrm{vec}^H(\mathrm{A})\mathrm{vec}(\mathrm{B})$, the second and third lines of (20) can be written as:

$$\begin{aligned}
&\boldsymbol{y}^H\begin{bmatrix}0 & 0\\ 0 & I_M\end{bmatrix}\boldsymbol{y} + \varpi_1^2 \geq 0,\\
&\boldsymbol{y}^H\begin{bmatrix}I_{ML} & 0\\ 0 & 0\end{bmatrix}\boldsymbol{y} + \varpi_3^2 \geq 0.
\end{aligned} \tag{22}$$

where $y = \mathrm{vec}(\begin{bmatrix}diag(\Delta\boldsymbol{h}_{2,k}^H)G\\ \Delta\boldsymbol{h}_{1,k}^H\end{bmatrix}^H)$.

Based on the definition $\mathrm{tr}(\mathrm{QPSK}) = \left(\mathrm{vec}(\mathrm{K})^H\right)^H(\mathrm{S}^{\mathrm{T}}\otimes\mathrm{Q})\mathrm{vec}(\mathrm{P})$, (20) can be written as:

$$\boldsymbol{y}^H\left(\bar{\boldsymbol{P}}\otimes\boldsymbol{S}\right)\boldsymbol{y} + 2\,\mathrm{Re}\left\{\mathrm{vec}^H\left(\boldsymbol{S}\begin{bmatrix}\mathrm{diag}(\bar{\boldsymbol{h}}_{2,k}^H)G\\ \bar{\boldsymbol{h}}_{1,k}^H\end{bmatrix}^H \bar{\boldsymbol{P}}\right)y\right\} + \mathrm{tr}\left(\boldsymbol{S}\begin{bmatrix}\mathrm{diag}(\bar{\boldsymbol{h}}_{2,k}^H)G\\ \bar{\boldsymbol{h}}_{1,k}^H\end{bmatrix}^H \bar{\boldsymbol{P}}\begin{bmatrix}\mathrm{diag}(\bar{\boldsymbol{h}}_{2,k}^H)G\\ \bar{\boldsymbol{h}}_{1,k}^H\end{bmatrix}\right) - c \geq 0 \tag{23}$$

Based on Lemma 1, (22) and (23) can be expressed as:

$$\begin{bmatrix}
\bar{\boldsymbol{P}}\otimes\boldsymbol{S} + \begin{bmatrix}\mu_1 I_{ML} & 0\\ 0 & \mu_2 I_{ML}\end{bmatrix} & \mathrm{vec}\left(\boldsymbol{S}\begin{bmatrix}\mathrm{diag}(\bar{\boldsymbol{h}}_{2,k}^H)G\\ \bar{\boldsymbol{h}}_{1,k}^H\end{bmatrix}^H \bar{\boldsymbol{P}}\right)\\
\mathrm{vec}^H\left(\boldsymbol{S}\begin{bmatrix}\mathrm{diag}(\bar{\boldsymbol{h}}_{2,k}^H)G\\ \bar{\boldsymbol{h}}_{1,k}^H\end{bmatrix}^H \bar{\boldsymbol{P}}\right) & tr\left(\boldsymbol{S}\begin{bmatrix}\mathrm{diag}(\bar{\boldsymbol{h}}_{2,k}^H)G\\ \bar{\boldsymbol{h}}_{1,k}^H\end{bmatrix}^H \bar{\boldsymbol{P}}\begin{bmatrix}\mathrm{diag}(\bar{\boldsymbol{h}}_{2,k}^H)G\\ \bar{\boldsymbol{h}}_{1,k}^H\end{bmatrix}\right) - c - \eta_1\varpi_3^2 - \eta_2\varpi_1^2
\end{bmatrix} \succeq 0 \tag{24}$$

where the relaxation variables $\eta_1 \geq 0, \eta_2 \geq 0$.

For the non-convex constraint C2, this subsection derives its lower bound via an identity:

$$\mathrm{tr}\left(\boldsymbol{A}\boldsymbol{S}\boldsymbol{A}^{\mathrm{H}}(\boldsymbol{Z})^{-1}\right) \geq \frac{\mathrm{tr}\left(\boldsymbol{A}\boldsymbol{S}\boldsymbol{A}^{\mathrm{H}}\right)}{\mathrm{tr}(\boldsymbol{Z})} \tag{25}$$

Hence, constraint C2 admits a more tractable approximation:

$$\mathrm{tr}\left(\boldsymbol{ASA}^{\mathrm{H}}\right)-\gamma_r\mathrm{tr}\left(\boldsymbol{Z}\right)\geq 0 \tag{26}$$

The reflection power constraint of IRS in C4 can be equivalent to:

$$\left\|\boldsymbol{\Xi}^{\mathrm{H}}\boldsymbol{Gw}\right\|_{\mathbf{F}}^{2}+\left\|\boldsymbol{\Xi Q\Xi}^{\mathrm{H}}\boldsymbol{Gw}\right\|_{\mathbf{F}}^{2}+\sigma_{\mathrm{I}}^{2}\mathrm{tr}\left(\boldsymbol{\Xi\Xi}^{\mathrm{H}}\right)-\mathrm{P}_{\mathrm{IRS}}\leq 0 \tag{27}$$

According to (24), (26), (27), the subproblem 1 can be equivalent to the following SDP problem:

$$\begin{aligned}&\max_{\boldsymbol{S}}\sum_{k}^{K}\log_2\left(1+\mathrm{tr}\left(\boldsymbol{Sh}_k\boldsymbol{h}_k^{\mathrm{H}}\right)/\boldsymbol{\varepsilon}\right)\\&s.t.\quad (24),(26),(27),\mathrm{C3}\\&\quad\boldsymbol{S}\succeq 0,rank(\boldsymbol{S})=1\end{aligned} \tag{28}$$

where $\boldsymbol{\varepsilon}=\sigma_{\mathrm{I}}^{2}\bar{\boldsymbol{h}}_{2,k}^{\mathrm{H}}\boldsymbol{\Xi\Xi}^{\mathrm{H}}\bar{\boldsymbol{h}}_{2,k}+\sigma_C^2$. Except for constraint $rank(S)=1$, the problem in (28) is a convex optimization problem. The problem can therefore be relaxed into an SDR formulation by discarding the rank-one constraint and subsequently solved using the CVX toolbox [37]. After solving (28) and obtaining the optimal solution, we first check its rank. If the rank equals one, the optimal beamforming vector can be directly recovered via eigenvalue decomposition. If the rank is greater than one [5,37], the rank-one decomposition theorem is employed to obtain the optimal weighting vector $\boldsymbol{w}$ for the DFRC system.

3.3. Optimizing the IRS reflection vector $\boldsymbol{p}$

The objective function (17) contains quartic functions of the reflection coefficient matrix $\boldsymbol{\Xi}$ in both constraints C2 and C4. To address this, we transform the high-order constraints into QCQP constraints via the MM algorithm, and jointly apply SDR and FP techniques to solve the non-convex objective function.

The fractional programming in the objective function of (17) can be resolved using the method from [39], and the optimization problem can be transformed as:

$$\begin{aligned}&\max_{\bar{\boldsymbol{P}}}\sum_{k}^{K}\log_2\left(1+2\boldsymbol{y}_{k,t}\sqrt{\mathrm{tr}\left(\bar{\boldsymbol{P}}\mathbf{H}\right)}-\boldsymbol{y}_{k,t}^{2}\boldsymbol{c}_1\right)\\&s.t.\quad (24),\mathrm{C2},\mathrm{C4},\mathrm{C5}\end{aligned} \tag{29}$$

where $\boldsymbol{H}=\begin{bmatrix}\mathrm{diag}(\boldsymbol{h}_{2,k}^{H})G\\ \boldsymbol{h}_{1,k}^{H}\end{bmatrix}^{H}\boldsymbol{S}\begin{bmatrix}\mathrm{diag}(\boldsymbol{h}_{2,k}^{H})G\\ \boldsymbol{h}_{1,k}^{H}\end{bmatrix}$, $\mathrm{c}_1=\sigma_{\mathrm{I}}^{2}tr\left(\left(\bar{\mathbf{h}}_{2,k}\bar{\mathbf{h}}_{2,k}^{H}\right)\odot\boldsymbol{P}_0\right)+\sigma_C^2$, $\boldsymbol{P}_0=\bar{\boldsymbol{P}}_{1:L,1:L}$. The auxiliary variable $\boldsymbol{y}_{k,t}$ is updated iteratively as:

$$\boldsymbol{y}_{k,t+1}=\frac{\sqrt{\mathrm{tr}\left(\bar{\boldsymbol{P}}\boldsymbol{H}\right)_t}}{\boldsymbol{c}_{1,t}} \tag{30}$$

where $\mathrm{tr}\left(\bar{\boldsymbol{P}}\boldsymbol{H}\right)_t$ and $\boldsymbol{c}_{1,t}$ are the results obtained at the t-th iteration.

To derive a surrogate function for the objective in (10), a lower bound of the objective function is obtained via first-order Taylor expansion under the MM framework [36], as shown in Lemma 2.

Lemma 2: The radar SINR can be minimized via the surrogate function at the t-th iteration, which is

$$\begin{aligned}\mathrm{tr}\left(\boldsymbol{X}^{\mathrm{H}}\left(\boldsymbol{Z}\right)^{-1}\boldsymbol{X}\right)\geq 2\mathrm{Re}\left(\mathrm{tr}\left(\boldsymbol{X}_t^{\mathrm{H}}\left(\boldsymbol{Z}\right)_t^{-1}\boldsymbol{X}\right)\right)\\-\mathrm{tr}\left(\left(\boldsymbol{Z}\right)_t^{-1}\boldsymbol{X}_t\boldsymbol{X}_t^{\mathrm{H}}\left(\boldsymbol{Z}\right)_t^{-1}\boldsymbol{Z}\right)\end{aligned}\tag{31}$$

where $\boldsymbol{X}_t$ and $\left(\boldsymbol{Z}\right)_t^{-1}$ denote the t-th iteration elements of auxiliary matrices $\boldsymbol{X}$ and $\boldsymbol{Z}$ respectively.

Based on Lemma 2, the lower bound of radar SINR at the t-th iteration is:

$$\begin{aligned}\mathrm{tr}\left(\boldsymbol{A}\boldsymbol{w}\boldsymbol{w}^{\mathrm{H}}\boldsymbol{A}^{\mathrm{H}}\left(\boldsymbol{Z}\right)^{-1}\right)\geq 2\mathrm{Re}\left(\mathrm{tr}\left(\boldsymbol{A}\boldsymbol{w}\boldsymbol{w}^{\mathrm{H}}\boldsymbol{A}_t^{\mathrm{H}}\left(\boldsymbol{Z}\right)_t^{-1}\right)\right)\\-\mathrm{tr}\left(\left(\boldsymbol{Z}\right)_t^{-1}\boldsymbol{A}_t\boldsymbol{w}\boldsymbol{w}^{\mathrm{H}}\boldsymbol{A}_t^{\mathrm{H}}\left(\boldsymbol{Z}\right)_t^{-1}\boldsymbol{Z}\right)\end{aligned}\tag{32}$$

According to property $\mathrm{tr}\left(\mathrm{A}^{\mathrm{H}}\mathrm{B}\right)=\left(\mathrm{vec}\left(\mathrm{A}\right)\right)^{\mathrm{H}}\mathrm{vec}\left(\mathrm{B}\right)$, the first right-hand term $2\mathrm{Re}\left(\mathrm{tr}\left(\boldsymbol{A}\boldsymbol{w}\boldsymbol{w}^{\mathrm{H}}\boldsymbol{A}_t^{\mathrm{H}}\left(\boldsymbol{Z}\right)_t^{-1}\right)\right)$ in (32) can be written as:

$$\begin{aligned}&2\mathrm{Re}\left(\mathrm{tr}\left(\boldsymbol{A}\boldsymbol{w}\boldsymbol{w}^{\mathrm{H}}\boldsymbol{A}_t^{\mathrm{H}}\left(\boldsymbol{Z}\right)_t^{-1}\right)\right)\\&=2\mathrm{Re}\left(\mathrm{tr}\left(\left(\boldsymbol{G}^{\mathrm{H}}\boldsymbol{\Xi}\boldsymbol{Q}\boldsymbol{\Xi}^{\mathrm{H}}\boldsymbol{G}+\mathbf{F}\right)\boldsymbol{S}\boldsymbol{A}_t^{\mathrm{H}}\left(\boldsymbol{Z}\right)_t^{-1}\right)\right)\\&=2\mathrm{Re}(\left(\mathrm{vec}\left(\boldsymbol{\Xi}^{\mathrm{H}}\boldsymbol{Q}^{\mathrm{H}}\boldsymbol{\Xi}\right)\right)^{\mathrm{H}}\mathrm{vec}\left(\boldsymbol{G}\boldsymbol{S}\boldsymbol{A}_t^{\mathrm{H}}\left(\boldsymbol{Z}\right)_t^{-1}\boldsymbol{G}^{\mathrm{H}}\right)\\&\quad+\left(\mathrm{vec}\left(\boldsymbol{F}^{\mathrm{H}}\right)\right)^{\mathrm{H}}\mathrm{vec}\left(\boldsymbol{S}\boldsymbol{A}_t^{\mathrm{H}}\left(\boldsymbol{Z}\right)_t^{-1}\right))\end{aligned}\tag{33}$$

In turn, (33) can be written as:

$$\begin{aligned}&2\mathrm{Re}\left(\mathrm{tr}\left(\boldsymbol{A}\boldsymbol{w}\boldsymbol{w}^{\mathrm{H}}\boldsymbol{A}_t^{\mathrm{H}}\left(\boldsymbol{Z}\right)_t^{-1}\right)\right)\\&=2\mathrm{Re}\left(\boldsymbol{p}_0^{\mathrm{H}}\boldsymbol{a}+\boldsymbol{b}\right)\end{aligned}\tag{34}$$

where $\boldsymbol{a}=\left(\mathrm{diag}\left(\mathrm{vec}\left(\boldsymbol{Q}^{\mathrm{H}}\right)\right)\right)^{\mathrm{H}}\mathrm{vec}\left(\boldsymbol{G}\boldsymbol{S}\boldsymbol{A}_t^{\mathrm{H}}\left(\boldsymbol{Z}\right)_t^{-1}\boldsymbol{G}^{\mathrm{H}}\right)$, $\boldsymbol{b}=\left(\mathrm{vec}\left(\boldsymbol{F}^{\mathrm{H}}\right)\right)^{\mathrm{H}}\mathrm{vec}\left(\boldsymbol{S}\boldsymbol{A}_t^{\mathrm{H}}\left(\boldsymbol{Z}\right)_t^{-1}\right)$, $\boldsymbol{p}_0=\mathrm{vec}\left(\boldsymbol{P}_0\right)$.

Since the beamforming vector $\boldsymbol{w}$ is constant in subproblem 2, C remains fixed, and the second term $tr\left(\left(\boldsymbol{Z}\right)_t^{-1}\boldsymbol{A}_t\boldsymbol{w}\boldsymbol{w}^{\mathrm{H}}\boldsymbol{A}_t^{\mathrm{H}}\left(\boldsymbol{Z}\right)_t^{-1}\boldsymbol{Z}\right)$ in (32) can be written as:

$$\begin{aligned}&\mathrm{tr}\left(\left(\boldsymbol{Z}\right)_t^{-1}\boldsymbol{A}_t\boldsymbol{w}\boldsymbol{w}^{\mathrm{H}}\boldsymbol{A}_t^{\mathrm{H}}\left(\boldsymbol{Z}\right)_t^{-1}\boldsymbol{Z}\right)\\&=\mathrm{tr}\left(\mathbf{C}\boldsymbol{Z}\right)\\&=\mu^2\mathrm{tr}\left(\mathbf{C}\boldsymbol{G}^{\mathrm{H}}\boldsymbol{\Xi}^{\mathrm{H}}\boldsymbol{G}\boldsymbol{S}\boldsymbol{G}^{\mathrm{H}}\boldsymbol{\Xi}\boldsymbol{G}\right)\\&\quad+\sigma_{\mathrm{I}}^2\mathrm{tr}\left(\mathbf{C}\boldsymbol{G}^{\mathrm{H}}\boldsymbol{\Xi}\boldsymbol{\Xi}^{\mathrm{H}}\boldsymbol{G}\right)+\sigma_{\mathrm{D}}^2\mathrm{tr}\left(\mathbf{C}\boldsymbol{I}_{\mathrm{M}}\right)\end{aligned}\tag{35}$$

where $\mathbf{C}=\left(\boldsymbol{Z}\right)_t^{-1}\boldsymbol{A}_t\boldsymbol{w}\boldsymbol{w}^{\mathrm{H}}\boldsymbol{A}_t^{\mathrm{H}}\left(\boldsymbol{Z}\right)_t^{-1}$.

The first term $\mu^2\mathrm{tr}\left(\mathbf{C}\boldsymbol{G}^{\mathrm{H}}\boldsymbol{\Xi}^{\mathrm{H}}\boldsymbol{G}\boldsymbol{S}\boldsymbol{G}^{\mathrm{H}}\boldsymbol{\Xi}\boldsymbol{G}\right)$ in (35) can be written as:

$$\begin{aligned}&\mu^2\mathrm{tr}\left(\mathbf{C}\boldsymbol{G}^{\mathrm{H}}\boldsymbol{\Xi}\boldsymbol{G}\boldsymbol{S}\boldsymbol{G}^{\mathrm{H}}\boldsymbol{\Xi}^{\mathrm{H}}\boldsymbol{G}\right)\\&=\mu^2\left(\mathrm{vec}\left(\boldsymbol{G}\boldsymbol{S}^{\mathrm{H}}\boldsymbol{G}^{\mathrm{H}}\right)\right)^{\mathrm{H}}\mathrm{vec}\left(\boldsymbol{G}\mathbf{C}\boldsymbol{G}^{\mathrm{H}}\odot\left(\boldsymbol{P}_0\right)\right)\\&=\mu^2\left(\mathrm{vec}\left(\boldsymbol{G}\boldsymbol{S}^{\mathrm{H}}\boldsymbol{G}^{\mathrm{H}}\right)\right)^{\mathrm{H}}\mathrm{diag}\left(\mathrm{vec}\left(\boldsymbol{G}\mathbf{C}\boldsymbol{G}^{\mathrm{H}}\right)\right)\mathrm{vec}\left(\boldsymbol{P}_0\right)\end{aligned}\tag{36}$$

(36) can be written as:

$$\mu^2 \mathrm{tr}\left(\mathbf{C}\boldsymbol{G}^{\mathrm{H}}\boldsymbol{\Xi}\boldsymbol{G}\boldsymbol{S}\boldsymbol{G}^{\mathrm{H}}\boldsymbol{\Xi}^{\mathrm{H}}\boldsymbol{G}\right)=\boldsymbol{d}\boldsymbol{p}_0 \tag{37}$$

where $\boldsymbol{d}=\mu^2\left(\mathrm{vec}\left(\boldsymbol{G}\boldsymbol{S}^{\mathrm{H}}\boldsymbol{G}^{\mathrm{H}}\right)\right)^{\mathrm{H}}\mathrm{diag}\left(\mathrm{vec}\left(\boldsymbol{G}\mathbf{C}\boldsymbol{G}^{\mathrm{H}}\right)\right)$.

Define $\boldsymbol{e}=\sigma_{\mathrm{I}}^2\mathrm{tr}\left(\boldsymbol{G}\mathbf{C}\boldsymbol{G}^{\mathrm{H}}\odot\boldsymbol{P}_0\right)$, (35) can be written as:

$$\mathrm{tr}\left(\mathbf{C}\boldsymbol{Z}\right)=\boldsymbol{d}\boldsymbol{p}_0+\boldsymbol{e} \tag{38}$$

The radar SINR is equivalently expressed as (39) using (34), (37), (38) and $\boldsymbol{g}$:

$$\mathrm{SINR}=2\mathrm{Re}\left(\boldsymbol{p}_0^{\mathrm{H}}\mathbf{a}+\mathrm{b}\right)-\boldsymbol{d}\boldsymbol{p}_0-\boldsymbol{e}-\boldsymbol{g} \tag{39}$$

where $\boldsymbol{g}=\sigma_{\mathrm{D}}^2\mathrm{tr}\left(\mathbf{C}\mathrm{I}_{\mathrm{M}}\right)$.

The fourth constraint C3 can be written as:

$$\mathrm{tr}\left(\boldsymbol{\Xi}\boldsymbol{Q}\boldsymbol{\Xi}^{\mathrm{H}}\boldsymbol{G}\boldsymbol{S}\boldsymbol{G}^{\mathrm{H}}\boldsymbol{\Xi}\boldsymbol{Q}^{\mathrm{H}}\boldsymbol{\Xi}^{\mathrm{H}}\right)+\mathrm{tr}\left(\boldsymbol{\Xi}^{\mathrm{H}}\boldsymbol{G}\boldsymbol{S}\boldsymbol{G}^{\mathrm{H}}\boldsymbol{\Xi}\right)+\sigma_{\mathrm{I}}^2\mathrm{tr}\left(\boldsymbol{\Xi}\boldsymbol{\Xi}^{\mathrm{H}}\right)-\mathrm{P}_{\mathrm{IRS}}\le 0 \tag{40}$$

According to property $\mathrm{tr}\left(\mathrm{QPSK}\right)=\left(\mathrm{vec}\left(\mathrm{K}\right)^{H}\right)^{H}\left(\mathrm{S}^{\mathrm{T}}\otimes\mathrm{Q}\right)\mathrm{vec}\left(\mathrm{P}\right)$, $\mathrm{tr}\left(\boldsymbol{\Xi}^{\mathrm{H}}\boldsymbol{Q}\boldsymbol{\Xi}\boldsymbol{G}\boldsymbol{S}\boldsymbol{G}^{\mathrm{H}}\boldsymbol{\Xi}^{\mathrm{H}}\boldsymbol{Q}^{\mathrm{H}}\boldsymbol{\Xi}\right)$ can be expressed as:

$$\begin{aligned}&\mathrm{tr}\left(\boldsymbol{\Xi}\boldsymbol{Q}\boldsymbol{\Xi}^{\mathrm{H}}\boldsymbol{G}\boldsymbol{S}\boldsymbol{G}^{\mathrm{H}}\boldsymbol{\Xi}\boldsymbol{Q}^{\mathrm{H}}\boldsymbol{\Xi}^{\mathrm{H}}\right)\\&=\left(\mathrm{vec}\left(\boldsymbol{\Xi}\boldsymbol{Q}^{\mathrm{H}}\boldsymbol{\Xi}^{\mathrm{H}}\right)\right)^{\mathrm{H}}\left(\mathbf{I}_{\mathrm{L}}\otimes\boldsymbol{G}\boldsymbol{S}\boldsymbol{G}^{\mathrm{H}}\right)\mathrm{vec}\left(\boldsymbol{\Xi}\boldsymbol{Q}^{\mathrm{H}}\boldsymbol{\Xi}^{\mathrm{H}}\right)\\&=\left\|\mathbf{J}\boldsymbol{p}_0\right\|_2^2\end{aligned} \tag{41}$$

where $\mathbf{J}=\boldsymbol{U}\mathrm{diag}\left(\mathrm{vec}\left(\boldsymbol{Q}^{\mathrm{H}}\right)\right)$ and $\left(\mathbf{I}_L\otimes\boldsymbol{G}\mathrm{S}\boldsymbol{G}^{\mathrm{H}}\right)=\boldsymbol{U}\boldsymbol{U}^{\mathrm{H}}$.

Following (41), equation (40) can be rewritten as:

$$\left\|\mathbf{J}\boldsymbol{p}_0\right\|_2^2+\boldsymbol{\zeta}-\mathrm{P}_{\mathrm{IRS}}\le 0 \tag{42}$$

where $\boldsymbol{\zeta}=\left(\boldsymbol{G}\mathbf{S}\boldsymbol{G}^{\mathrm{H}}\right)\odot\boldsymbol{P}_0+\sigma_{\mathrm{I}}^2\mathrm{tr}(\boldsymbol{P}_0)$.

According to (24)、(39)、(42) , the above optimization problem can be transformed into a SDR problem:

$$\begin{aligned}&\max_{\bar{\boldsymbol{P}}}\ \sum_{k}^{K}\log_2\left(1+2\mathrm{y}_{k,t}\sqrt{\mathrm{tr}\left(\bar{\boldsymbol{P}}\mathbf{H}\right)}-\mathrm{y}_{k,t}^2c_1\right)\\&s.t.\quad (24),(39),(42)\\&\qquad \mathrm{C4}:\ \bar{\boldsymbol{P}}_{l,l}=1,\ \ l=1,...,\mathrm{L}\\&\qquad \mathrm{C5}:\ \bar{\boldsymbol{P}}\succeq 0\end{aligned} \tag{43}$$

The optimization problem in (43) is convex and can be solved using the CVX toolbox [37]. The overall optimization algorithm of this paper is summarized in Algorithm 1, and thresholds ε_1 and ε_2.

In (28), the number of variables is $m_1=M^2$, and its approximate computational complexity is:

$$o_1 = o\left(\left(K\left(ML+1\right)+M+2\right)^{1/2} m_1\left(m_1^2 + m_1\left(K\left(ML+1\right)^2 + M^2\right)\right) + \left(K\left(ML+1\right)^3 + M^3\right) + M^2\right) \approx o\left(K^{3.5}L^{3.5}M^{6.5}\right) .$$

Similarly, the approximate computational complexity of optimization problem (43) is $o_2 = o\left(K^{3.5}M^{3.5}L^{6.5}\right)$ [36]. Therefore, the overall computational complexity of the proposed algorithm is $\mathbf{I}_1\left(o_1 + \mathbf{I}_2 o_2\right)$.

Algorithm 1: SDR-FP-based AO Algorithm

Input： $\mathrm{M, L, K, y}_{k,t}, \gamma_r, \gamma_c, \varepsilon_1, \varepsilon_2, \sigma_{\mathrm{D}}^2, \sigma_{\mathrm{C}}^2, \sigma_{\mathrm{I}}^2$,

1. Decompose objective function (17) into two subproblems.
2. Transform inequality constraint C1 into finite constraints via Lemma 1.
3. Derive surrogate function (39) for constraint C2 using Lemma 2.
4. Introduce auxiliary variable $\mathrm{y}_{k,t}$ to obtain FP form of objective function in (29).
5. Reformulate into tractable subproblems (28) and (43) through algebraic operations
6. Initialize matrices： $\boldsymbol{S}, \bar{\boldsymbol{P}}$, j=0, i = 0
7.Repeat
8. Obtain $\boldsymbol{S}$ by solving (28) with given $\bar{\boldsymbol{P}}$
9. Repeat
10. Obtain $\bar{\boldsymbol{P}}$ by solving (43) with given $\boldsymbol{S}$
11. $j = j+1$
12. Until $\left|R_U(j+1) - R_U(j)\right| \le \varepsilon_1$
13. $i = i+1$
14. Until $\left|R_U(i+1) - R_U(i)\right| \le \varepsilon_2$,

Output： R_U

4. Simulation analysis

The simulation parameters are configured as follows: the DFRC transmitter employs M=6 antennas, K=2 communication ships are served, with a self-interference coefficient of 0.1[40]. The DFRC transmitter utilizes a uniform linear array with half-wavelength spacing, as illustrated in Fig. 2. The coordinates of the DFRC transmitter, the IRS-mounted unmanned surface vehicle, and the target are set to [0,0], [40,40], and [80,20], respectively. The K communication ships are randomly distributed within a circular area centered at [20,10] with a radius of 5. Additional parameters are specified below: $\sigma_{\mathrm{C}}^2, \sigma_{\mathrm{D}}^2, \sigma_{\mathrm{I}}^2$ are all set to σ , $\sigma_1 = -90\mathrm{dBm}$, $\sigma_2 = -70\mathrm{dBm}$.

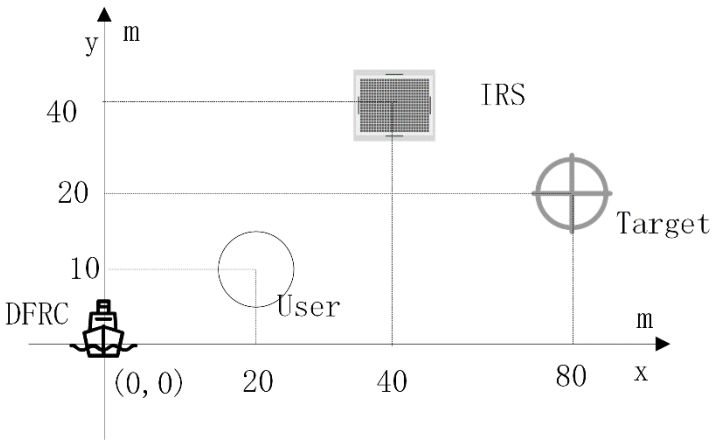

Fig. 2 The simulation system

A. The influence of the number of algorithm iterations on the sum and rate

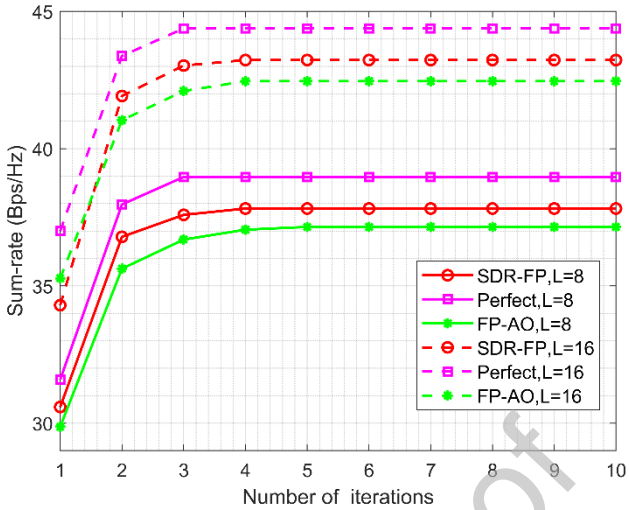

Fig. 3 Algorithm convergence graph

Fig. 3 presents the convergence performance of the proposed algorithm, the FP-AO algorithm in [29], and the case with perfect CSI for comparison. This analysis assumes an ideal low-noise environment with $\sigma = \sigma_1$, where both communication ships and radar detection maintain 10dB SINR thresholds. The DFRC transmitter operates under 1W maximum transmit power and 0.1W maximum reflection power. To assess convergence under varying IRS configurations, two reflecting element counts L=8 and 16 were evaluated. Fig. 3 illustrates that the proposed algorithm begins to converge at the fourth iteration, which effectively validates its feasibility. Therefore, the number of simulation iterations is set to four. Although the optimization performance of the proposed algorithm is lower than that under perfect CSI due to channel uncertainty, it achieves higher communication rates compared to the FP-AO algorithm. This improvement results from the effective mitigation of self-interference signals in the DFRC-IRS-DFRC link. Furthermore, the incorporation of an inner-loop subroutine accelerates convergence, yielding faster convergence rates than FP-AO.

B. The influence of DFRC transmit power on the sum rate

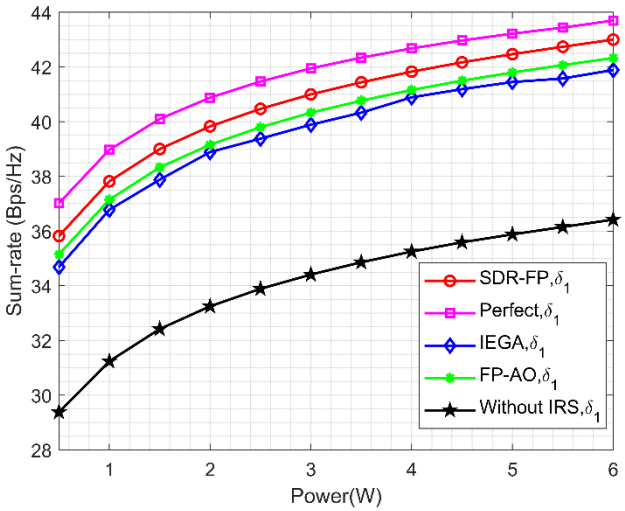

Fig. 4 Communication sum-rate and transmit power

Fig. 4 shows the effect of DFRC transmit power on both communication and sensing rates. As illustrated, user communication performance improves with increasing transmit power since higher power enhances signal energy through both direct and reflected paths. The non-IRS-assisted case exhibits significantly lower sum rate than other methods, demonstrating how IRS dynamically reconfigures the propagation environment to increase spatial degrees of freedom and compensate for direct path limitations. The "IEGA" label denotes the Improved Elitist Genetic Algorithm (IEGA) from [35], which relies on stochastic search and evolutionary operations that struggle to balance communication-radar resource demands. To maintain convergence speed, IEGA employs an elitist strategy with small population size, resulting in suboptimal performance inferior to our method. Furthermore, increasing DFRC transmit power yields negligible improvement in radar performance gap between methods due to saturation effects from environmental clutter and system noise beyond certain power levels.

C. The influence of the number of IRS reflection units on the sum rate

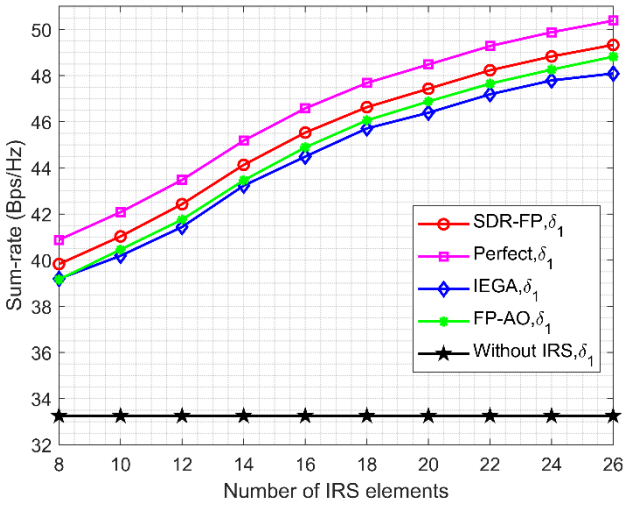

Fig. 5 Communication sum rate and the number of IRS reflection units

Fig. 5 illustrates the relationship between sum rate and IRS element count with SINR thresholds for both communication ships and radar set at 10dB, and DFRC transmit power fixed at 2W. As demonstrated, the sum rate exhibits significant enhancement with increasing IRS elements due to dual physical mechanisms: expanded element count enables greater capture and reflection of electromagnetic energy from the DFRC transmitter, thereby boosting array gain. Simultaneously, passive beamforming via phase shifters optimizes spatial directivity of reflected beams, generating focused radiation toward target communication ships that further strengthens channel conditions. The "Without IRS" scenario remains constant since it lacks IRS assistance. Our method outperforms FP-AO in optimized sum rate through integrated self-interference cancellation. Furthermore, as the number of reflecting elements increases, both the proposed method and the FP-AO algorithm progressively outperform the IEGA algorithm. This is because the algorithmic complexity rises with the number of reflecting elements, while the IEGA algorithm employs a relatively small population size, leading to a significant decline in optimization performance under high-complexity conditions.

D. The influence of noise environment on the sum rate

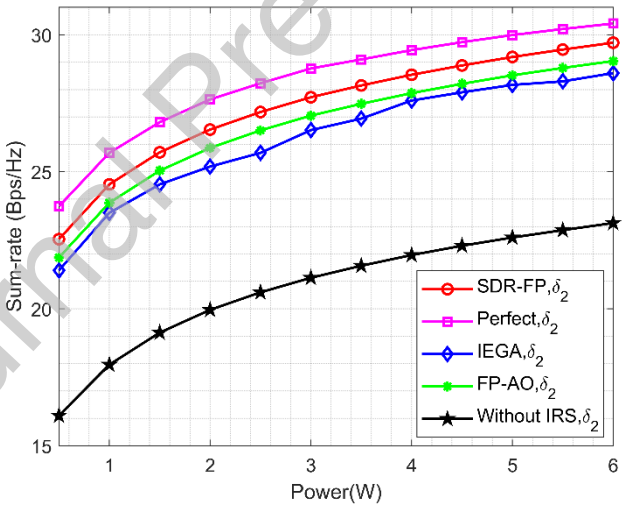

Fig. 6 Communication sum-rate in high-noise environment

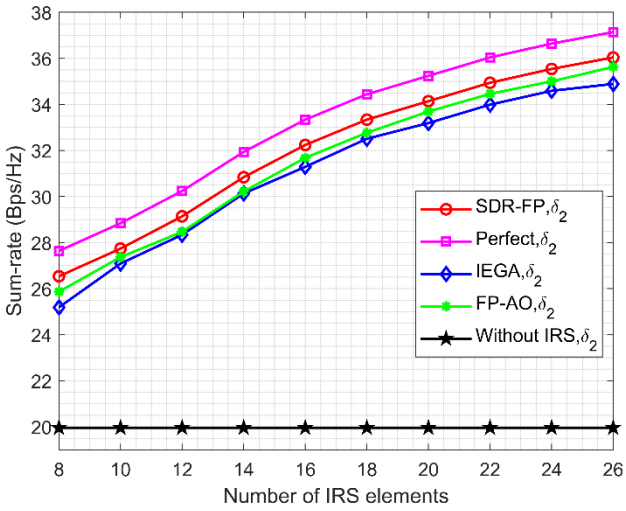

Fig. 7 Communication sum-rate in high-noise environment

Fig. 6 and Fig.7 respectively illustrate the trends of the total communication rate of the communication vessels versus the DFRC transmit power and the number of IRS reflecting elements under high noise interference conditions. In the simulation setup, the SINR threshold for both communication ships and radar is set to 10 dB, and the DFRC transmit power is fixed at 2 W. Analysis reveals that while noise degrades overall system performance, the proposed algorithm consistently approaches perfect-CSI optimization effectiveness in this noisy setting. Crucially, its performance enhancement trend with increasing transmit power and reflecting elements remains consistent with low-noise conditions, exhibiting no fundamental alteration despite intensified noise. This key observation demonstrates our algorithm's superior robustness against strong noise interference.

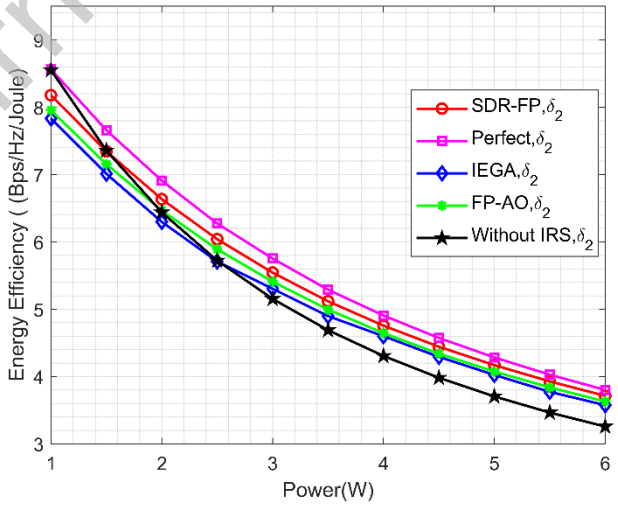

Fig. 8 Energy efficiency and DFRC transmit power

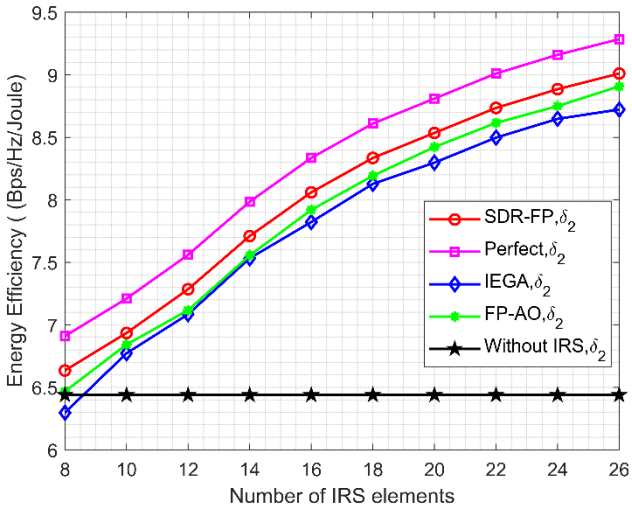

Fig. 9 Energy efficiency and the number of IRS elements

E. The influence of power and the number of reflection units on energy efficiency

Fig. 8 shows the impact of transmit power on the communication energy efficiency of the DFRC system [29]. The simulation conditions are the same as those in Fig. 6. As shown, all schemes exhibit a monotonic decreasing energy efficiency trend with increasing transmit power. This fundamental behavior stems from our core optimization objective focusing exclusively on maximizing communication sum rate without directly incorporating energy efficiency as an optimization variable. In low-power regions, the "Without IRS" scheme demonstrates comparable energy efficiency to our proposed method. However, as transmit power escalates, its efficiency rapidly deteriorates due to the absence of IRS gain, falling significantly below all IRS-assisted schemes. The performance of IEGA scheme depends on the population size and the number of iterations, and the global search ability is insufficient in high complexity scenarios, resulting in unsatisfactory energy efficiency. Crucially, even when fully accounting for IRS power consumption, our algorithm maintains energy efficiency closest to perfect-CSI cases, robustly validating its superiority in optimizing energy utilization by effectively balancing communication enhancement with power management.

Fig. 9 illustrates the effect of the number of IRS reflecting elements on the system's communication energy efficiency. The simulation settings are consistent with those in Fig.7. As illustrated, the proposed and benchmark algorithms exhibit energy efficiency versus element count trends that strongly correlate with those for sum-rate in Fig. 6, since our solution prioritizes and fully utilizes all available energy resources to maximize communication sum rate. Consequently, energy efficiency curves inherit fundamental characteristics aligned with this primary optimization objective. All optimized methods progressively outperform the "Without IRS" scheme with increasing elements, further demonstrating IRS assistance significantly enhances energy efficiency. Moreover, under identical high-noise interference, our method consistently maintains superior energy efficiency over comparative algorithms.

These results concurrently validate the algorithm's effectiveness in optimizing communication performance and its excellence in improving system energy utilization efficiency.

F. The influence of radar SINR constraint on sum rate

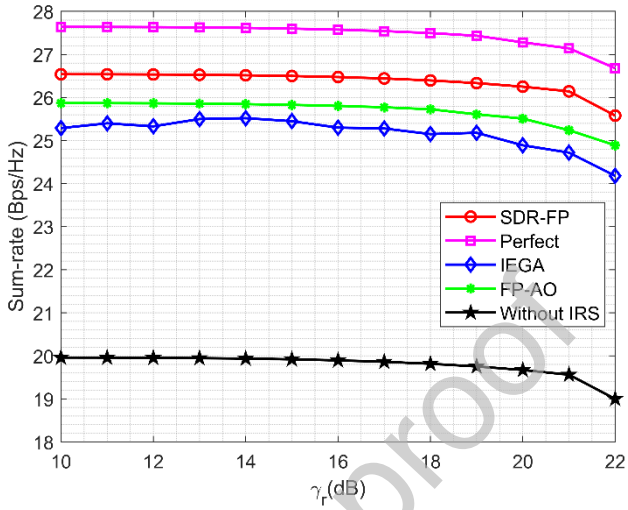

Fig. 10 Communication sum-rate and radar SINR threshold

Fig.10 shows the impact of the SINR requirement for radar detection on communication performance and rate, with radar SINR varying between 10–22dB, DFRC maximum transmit power fixed at 2W, and IRS reflecting elements set to 8. As shown, the communication sum rate decreases with increasing SINR due to competitive power allocation: higher radar SINR thresholds force the DFRC transmitter to allocate greater power for radar beamforming and transmission to satisfy enhanced detection performance. Consequently, power resources available for multi-ship data transmission diminish, directly reducing system sum rate. The performance gap between our method and the "Without IRS" scheme widens progressively with rising SINR thresholds, as beamforming matrix optimization faces stricter constraints without IRS assistance. At the 22dB threshold, our method maintains superior communication performance by leveraging supplementary propagation paths provided by the IRS for joint communication and detection, validating IRS effectiveness in enhancing DFRC system capabilities.

5. Conclusion

In this paper, an IRS-assisted shipborne DFRC system is investigated. The study focuses on the joint optimization of the active beamforming vector at the DFRC transmitter and the passive beamforming vector at the IRS. To address this problem, an AO algorithm based on SDR-FP is proposed. The method decomposes the optimization problem into subproblems, transforms quartic non-convex subproblems into tractable QCQP formulations via the MM framework, and solves them iteratively. For CSI uncertainty in dynamic maritime

environments, bounded channel error models represent imperfect CSI. Simulations demonstrate that under identical parameters, our algorithm outperforms IEGA and PF-AO in both low-noise and high-noise regimes. In future work, we will consider scenarios involving targets with larger dynamic ranges and more complex motion patterns, as well as multi-target detection in dynamic maritime environments.

References

[1] L. Zheng, M. Lops, Y. C. Eldar and X. Wang, "Radar and Communication Coexistence: An Overview: A Review of Recent Methods," in IEEE Signal Processing Magazine, vol. 36, no. 5, pp. 85-99, Sept. 2019.

[2] D. Li, B. Tang and L. Xue, "Waveform Design for MIMO DFRC Systems: Finer Sensing and Safer Communications," in IEEE Transactions on Signal Processing, vol. 72, pp. 4509-4524, 2024.

[3] W. Zheng, J. Shi, Y. Li, Z. Huang, Z. Zhang and Z. Li, "D ^{2} AF-Net: A Dual-Domain Adaptive Fusion Method for Radar Deception Jamming Recognition," in IEEE Transactions on Aerospace and Electronic Systems, 2025.

[4] R. Xu, R. Wen, G. Li, et al. "Interference suppression and low complexity communication reception for OOK-chirp based RCC system." Signal Processing, vol.220:109460, July 2024.

[5] Q. Chen, C. Huang, J. Shi, Z. Li and Q. Zhou, "Robust Co-Design of Transmit Waveform and Receive Filter for LPI FDA-MIMO Radar in Clutter and Jamming Environments," in IEEE Transactions on Aerospace and Electronic Systems, 2025.

[6] H. Zhang, W. Liu, Q. Zhang and B. Liu, "Joint Customer Assignment, Power Allocation, and Subchannel Allocation in a UAV-Based Joint Radar and Communication Network," in IEEE Internet of Things Journal, vol. 11, no. 18, pp. 29643-29660, Sept. 2024.

[7] L. Geng, Y. Li, L. Dong, et al. "Improving waveform for FDA-MIMO-based DFRC systems by collaborating modulation and optimization." Signal Processing, 2026, 238: 110158.

[8] A. Hassanien, M. G. Amin, E. Aboutanios and B. Himed, "Dual-Function Radar Communication Systems: A Solution to the Spectrum Congestion Problem," in IEEE Signal Processing Magazine, vol. 36, no. 5, pp. 115-126, Sept. 2019.

[9] A. Hanif, S. Ahmed, M. -S. Alouini and T. Y. Al-Naffouri, "Exploring the Synergy: A Review of Dual-Functional Radar Communication Systems," in IEEE Aerospace and Electronic Systems Magazine, March 2025.

[10] J. Zhu, W. Li, et al. "Waveform design of DFRC system for target detection in clutter environment," IEEE Signal Processing Letters, vol. 30, pp. 1517- 1521, October 2023.

[11] Z. Zhang and J. Tao. "Joint Beamforming Design for Radar and Multiple Communication Users in DFRC System, "Digital Signal Processing, vol. 159, 105010, April 2025.

[12] B. Guo, J. Liang, G. Wang, et al. "Bistatic MIMO DFRC system waveform design via fractional programming," IEEE Transactions on Signal Processing, vol. 71, pp. 1952- 1967, May 2023.

[13] C. Huang, Z. Huang, Q. Zhou, et al. "Joint Transmit Waveform and Receive Filter Design for the DFRC System with Imperfect CSI," IEEE Transactions on Radar Systems, vol. 2, pp. 288- 302, February 2024.

[14] L. Chen, Z. Wang, Y. Du, Y. Chen and F. R. Yu, "Generalized Transceiver Beamforming for DFRC with MIMO Radar and MU-MIMO Communication," in IEEE Journal on Selected Areas in Communications, vol. 40, no. 6, pp. 1795-1808, June 2022.

[15] L. Chen, X. Qin, Y. Chen and N. Zhao. "Joint waveform and clustering design for coordinated multi-point DFRC systems," IEEE Transactions on Communications, vol. 71, no. 3, pp. 1323- 1335, March 2023.

[16] D. Bao and R. Guo, "A Dual Function Intelligent Reflecting Surface in Integrated Radar Communication System," in IEEE Transactions on Intelligent Transportation Systems, vol. 26, no. 3, pp. 3471-3481, March 2025.

[17] R. Liu, M. Li, Y. Liu, Q. Wu and Q. Liu, "Joint Transmit Waveform and Passive Beamforming Design for RIS-Aided DFRC Systems," in IEEE Journal of Selected Topics in Signal Processing, vol. 16, no. 5, pp. 995-1010, Aug. 2022.

[18] Z. Zhu, M. Ning, G. Sun, et al. "The Interplay of DMA and RIS for Near-Field Integrated Sensing and Symbiotic Radio Systems," in IEEE Internet of Things Journal, vol. 12, no. 15, pp. 29529-29539, Aug. 2025.

[19] Y. Zhang, H. Ren, C. Pan, et al. "Secure Wireless Communication in Active RIS-Assisted DFRC Systems," in IEEE Transactions on Vehicular Technology, vol. 74, no. 1, pp. 626-640, Jan. 2025.

[20] Y. Zhang et al., "Secure Wireless Communication in Active RIS-Assisted DFRC Systems," in IEEE Transactions on Vehicular Technology, vol. 74, no. 1, pp. 626-640, Jan. 2025.

[21] B. Wang, H. Li, S. Shen, Z. Cheng and B. Clerckx, "A Dual-Function Radar-Communication System Empowered by Beyond Diagonal Reconfigurable Intelligent Surface," in IEEE Transactions on Communications, vol. 73, no. 3, pp. 1501-1516, March 2025.

[22] Z. Zhu, Z. Li, Z. Chu, et al. "Intelligent Reflecting Surface Assisted mmWave Integrated Sensing and Communication Systems," in IEEE Internet of Things Journal, vol. 11, no. 18, pp. 29427-29437, Sept. 2024.

[23] Z. Zhu, K. Guo, Z. Chu, et al. "Unlocking Integrated Wireless Powered Sensing and Communication Networks using Reconfigurable Intelligent Surface," in IEEE Transactions on Wireless Communications, 2025.

[24] L. Chen, J. Zhu, Y. Zou, Y. Lou and Y. Li, "STAR-RIS-Assisted Multicast Communications in DFRC-UAV-Enabled ISAC Systems," in IEEE Communications Letters, vol. 29, no. 1, pp. 170-174, Jan. 2025.

[25] M. Hua, Q. Wu, C. He, S. Ma and W. Chen, "Joint Active and Passive Beamforming Design for IRS-Aided

Radar-Communication," in IEEE Transactions on Wireless Communications, vol. 22, no. 4, pp. 2278-2294, April 2023.

[26] Z. Zhu, M. Gong, M. Zhang, et al. "Reinforcement Learning Based Resource Allocation in IRS Assisted SWIPT Systems," in IEEE Transactions on Vehicular Technology, vol. 74, no. 4, pp. 6790-6794, April 2025.

[27] B. Deng, Z. Yuan, Z. Tang, W. Jiao, C. Li and W. Zhou, "Energy Efficiency Optimization in IRS-Aided Multiuser MISO Communication Systems," in IEEE Sensors Journal, vol. 24, no. 21, pp. 35801-35808, Nov. 2024.

[28] W. Du et al., "Weighted Sum-Rate and Energy Efficiency Maximization for Joint ITS and IRS Assisted Multiuser MIMO Networks," in IEEE Transactions on Communications, vol. 70, no. 11, pp. 7351-7364, Nov. 2022.

[29] W. Zhong, Z. Yu, Y. Wu, F. Zhou, Q. Wu and N. Al-Dhahir, "Resource Allocation for an IRS-Assisted Dual-Functional Radar and Communication System: Energy Efficiency Maximization," in IEEE Transactions on Green Communications and Networking, vol. 7, no. 1, pp. 469-482, March 2023.

[30] F. S. Alqurashi, A. Trichili, N. Saeed, B. S. Ooi and M. -S. Alouini, "Maritime Communications: A Survey on Enabling Technologies, Opportunities, and Challenges," in IEEE Internet of Things Journal, vol. 10, no. 4, pp. 3525-3547, Feb. 2023.

[31] Z. Zhou, N. Ge, W. Liu and Z. Wang, "RIS-Aided Offshore Communications with Adaptive Beamforming and Service Time Allocation," ICC 2020 - 2020 IEEE International Conference on Communications (ICC), Dublin, Ireland, 2020, pp. 1-6.

[32] K. Li, M. Cui, G. Zhang, Q. Wu, D. Li, J. He. "Robust transmit and reflect beamforming design for IRS-assisted offshore NOMA communication systems, "IEEE Transactions on Vehicular Technology, vol. 73, no. 1, pp. 783 - 798, August 2023.

[33] W. Xu and L. Gu. "Energy-efficient resource optimization for IRS-assisted VLC-enabled offshore communication system." Journal of Marine Science and Engineering, vol. 12, no. 5: 772., March 2023.

[34] X. Cao, X. Hu and M. Peng. "Joint mode selection and beamforming for IRS-aided maritime cooperative communication systems," IEEE Transactions on Green Communications and Networking, vol. 7, no. 1, pp. 57 - 69, March 2023.

[35] X. Cao, S. Wang and Y. Zhang. "Intelligent Reflecting Surface Enhanced Maritime Joint Sensing and Communication Systems: Performance Optimization." IEEE Transactions on Communications, vol. 73, no. 2, pp. 938-949, March 2023.

[36] Z. Yu, H. Ren and C. Pan, et al. "Active RIS-aided ISAC systems: Beamforming design and performance analysis," IEEE Transactions on Communications, vol. 72, no. 3, pp. 1578 - 1595, March 2024.

[37] Z. M. Jiang, M. Rihan, P. Zhang, et al. "Intelligent reflecting surface aided dual-function radar and communication system," IEEE Systems Journal, vol. 16, no. 1, pp. 1578 - 1595, March 2022.

[38] L. Zheng, M. Lops and X. Wang, et al. "Joint design of overlaid communication systems and pulsed radars," IEEE Transactions on Signal Processing, vol. 66, no. 1, pp. 139 - 154, January 2018.

[39] K. Shen and W. Yu, "Fractional Programming for Communication Systems—Part I: Power Control and Beamforming," in IEEE Transactions on Signal Processing, vol. 66, no. 10, pp. 2616-2630, May 2018.

[40] Z. Peng, Z. Zhang, C. Pan, L. Li and A. L. Swindlehurst, "Multiuser Full-Duplex Two-Way Communications via Intelligent Reflecting Surface," in IEEE Transactions on Signal Processing, vol. 69, pp. 837-851, 2021.